Visual Abstract

Numerical simulation of dynamic mechanical properties of concrete based on 3D mesoscale model

Fengyan Qin
Architecture and Civil Engineering, West Anhui University, Lu'an 237012, China
qinfengyan1207@163.com

Jingsong Cheng, Heming Wen
CAS Key Laboratory for Mechanical Behavior and Design of Materials University of Science and Technology of China, Hefei 230026, China
hmwen@ustc.edu.cn

Hongbo Liu
School of Civil Engineering and Architecture, Heilongjiang University, Harbin 150080, China
HLiu@ hlju.edu.cn

ABSTRACT. This paper attempts to disclose the mechanical properties of concrete under dynamic load. To this end, concrete was considered as a three-phase composite of mortar, aggregate and interfacial transition zone (ITZ) on the mesoscale. In light of the dynamic constitutive relation of concrete, the dynamic response of concrete specimens was numerically simulated on a 3D meso-mechanical model. Then, the authors discussed how the loading speed, aggregate volume content, and aggregate particle size affect the dynamic mechanical properties of concrete. The simulation results show that the damage morphology of concrete under dynamic load agrees well with that of theoretical analysis; the peak stress of concrete increased with the loading speed, revealing an obvious strain rate enhancement effect; the peak stress of concrete also increased with aggregate volume content; however, the peak stress of concrete gradually decreased with the increase in aggregate particle size under the constant volume content and grading of aggregate. The research findings shed new light on anti-impact design of concrete structures.

KEYWORDS. Concrete; Dynamic Mechanical Properties; 3D Meso-Mechanical Model; Dynamic Constitutive Relation; Numerical Simulation; Peak Stress.

OPEN ACCESS

Citation: Qin, F., Cheng, J., Wen, H., Liu, H., Numerical simulation analysis of the dynamic mechanical property of concrete based on 3D meso-mechanical model, Frattura ed Integrità Strutturale, 45 (2018) 1-13.

Received: 15.03.2018
Accepted: 02.06.2018
Published: 01.07.2018

INTRODUCTION

Concrete is one of the most popular materials in structural engineering. It has been extensively applied in buildings, bridges, mines, dams, power plants and transport facilities. In addition to normal static load, all these engineering structures may be subject to such dynamic loads as earthquakes, vehicle vibration, engineering blasting and debris flow. Heavy losses of life and property may occur if the concrete of these structures fails or collapses under these loads. Considering the high incidence of earthquakes and debris flows in China, it is very meaningful to examine the mechanical properties of concrete under dynamic load.

There are obvious differences in macro strength and deformation features of concrete under dynamic load and that under static load. The dynamic load-induced response is a rather complex process, involving the evolution of microdefects in the material, the sensitive effect of material strain rate, and the impact of hydrostatic pressure correlation [1-5]. Under dynamic load, the change in concrete deformation and stress is often transmitted in the form of wave, featuring strong instantaneity. It is very difficult to observe the mesoscale destruction or explain the enhancement of mechanical parameters (e.g. concrete strength) through experimental research.

By contrast, the deformation, stress change and damage morphology during the impact can be visually presented through numerical simulation, which can provide some guidance on the cost and effect of the experiment. The numerical simulation of dynamic response starts from the microstructure of concrete. In general, a numerical model should be established based on theoretical and experimental results. Then, the macro-mechanical properties of the material and the destruction process of concrete can be explored against the microstructure. On the mesoscale, concrete can be regarded as a composite of mortar, aggregate, and the interfacial transition zone (ITZ).

Over the years, many micro-mechanical models have been developed, including but not limited to lattice model [6-7], stochastic particle model [8-9], random aggregate model [10-11], and random mechanical property model [12-13]. Based on meso-mechanical models, the numerical simulation can partially replace experimental research, provided that the models are rational and concrete parameters are precise enough. Nevertheless, the application of numerical simulation has been severely restricted by the lack of experimental data on the mechanical parameters of mortar, aggregate and the ITZ, and the low computing efficiency of 3D analytical models.

Much research has been done on the dynamic features of concrete at home and abroad. For example, Liu Haifeng et al. [14-19] investigated the mechanical properties and constitutive models of concrete under dynamic load, and simulated the dynamic features of concrete under the load using the Holmquist–Johnson–Cook (HJC) model. Du Xiuli et al. [20-21] subdivided the finite-element grids by characteristic unit scale method and projected the grids to the established random aggregate model. In this way, the random multi-scale mechanical model was created and applied to reveal the micro failure mechanism of concrete under dynamic load. Ren Wenyuan et al. [22] proposed to simulate the constituent materials of concrete in each phase with the micro finite-element model (FEM) based on X-ray computed tomography (XCT) images. Park et al. [23] conducted finite-element simulation of concrete and mortar at high strain rate, and analysed the bearing capacity, energy absorption and microstructure of the two materials under dynamic load.

According to the aggregate grading curve of concrete, Wang Zongmin et al. [24] generated random aggregates by Monte Carlo method, prepared tensile test specimens with single-edge cracks from the aggregates, and simulated the whole process of the rupture failure of these specimens. Considering the random aggregate structure of concrete, Ma Huaifa et al. [25] put forward a 3D meso-mechanical numerical model that reflects the random aggregate distribution or random mechanical properties of material in each phase. Song Laizhong et al. [26] ensured the rationality of aggregate distribution through random placement of parameterized aggregates, thereby fulfilling the bulk mass, fully-grade, high-strength requirements of aggregate arrangement simulation. By means of light gas gun, Zhang Zhu et al. [27] tested the dynamic mechanical properties test of concrete at different loading speeds, and then performed a numerical simulation on ANSYS Autodyn. The simulation results were contrasted with the experimental data to explain the wave propagation during the destruction of the flyer and the target plate.

There are only a few reports on how the size, distribution and volume content of aggregate on the dynamic mechanical properties of concrete. Taking concrete as two-phase heterogenous composite of aggregate and mortar, Liu Haifeng et al. [16-19] wrote a random distribution program of 2D spherical aggregate of concrete in ANSYS parametric design language (APDL), using Fuller's grading curve and Walraven plane transformation formula, and employed the program to discuss the effects of aggregate particle size, distribution and volume content on the dynamic mechanical properties of concrete. Xu et al. [28] assumed concrete as a three-phase heterogeneous composite of mortar, aggregate and the ITZ, identified the regularity of aggregate grading and particle size distribution according to Fuller's grading curve, and developed a random distribution program of 3D spherical aggregate of concrete in ANSYS APDL. Since the ITZ is too thin to simulate, the

aggregate was meshed into grids, the ITZ was generated by unit reconfiguration, and a 3D micro-mechanical model was created for concrete. The established model enjoys high computing efficiency.
In this paper, the dynamic concrete features are simulated at different loading speeds, aggregate volume contents and aggregate particle sizes, using the 3D micro-mechanical model proposed by Xu et al., and the influence rule of different factors on the dynamic mechanical properties of concrete are discussed in details. The mortar, aggregate and the ITZ were built on the material constitutive relation provided by Xu and Wen [29] and embedded in the business software ANSYS LS-DYNA for numerical simulation.

ESTABLISHMENT OF THE MESO-MECHANICAL MODEL

As mentioned above, the ANSYS LS-DYNA dynamic analysis software was adopted to simulate the response of concrete with randomly distributed 3D aggregate under dynamic load. As shown in Fig. 1, the test specimens are 100mm, 150mm or 200mm in side length. The upper and lower rigid plates respectively act as an actuator and a support, while the part between them is the concrete sample. The load was imposed onto the upper rigid plate to simulate concrete damage.

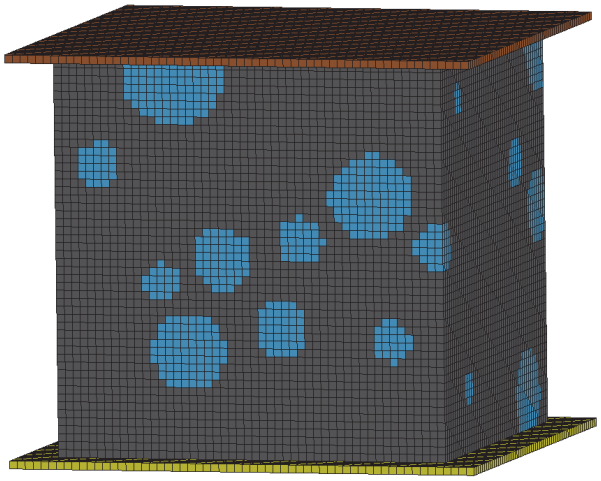

Figure 1: 3D meso-mechanical model.

Grid size

Both mortar and aggregate were simulated with the 3D entity unit of the same shape. The grid size was set to 2mm according to the side lengths of the cubic test specimens. Compared to mortar, the ITZ is a weak, porous, nonuniform thin layer wrapped in the outer surface of aggregate particles. The typical thickness of the ITZ is merely 10~50μm, which limits the minimum grid size. To improve the computing efficiency, 3D shell units were introduced to simulate the ITZ. Here, it is assumed that the ITZ consists of homogeneous materials and its thickness is the average of the maximum and minimum values: 30μm.

Distribution of aggregate particle size

Considering the effect of aggregate grading on the mechanical behaviour of concrete, Fuller's grading curve was adopted in our model to optimize concrete compactness and strength. The curve can be expressed as [30]:

$$P(d)=\left(\frac{d}{d_{\max}}\right)^{n} \tag{1}$$

where $P(d)$ is the cumulative percentage of aggregates passing a sieve with aperture diameter d; $d_{\max}$ is the maximum size of aggregate particle; n is the shape parameter of the gradation curve and ranges from 0.45 to 0.7. In this paper, n is taken as a common value of 0.5.

If the aggregate particle size distribution obeys Fuller's gradation curve, then the amount of aggregate within the grading segment $[d_s, d_{s+1}]$ can be obtained as:

$$V_{\text{agg}}\left[d_s, d_{s+1}\right] = \frac{P\left(d_{s+1}\right) - P\left(d_s\right)}{P\left(d_{\max}\right) - P\left(d_{\min}\right)} V_{\text{a}} V_{\text{all}} \tag{2}$$

where $V_{agg}[d_s, d_{s+1}]$ is the aggregate volume within the grading segment $[d_s, d_{s+1}]$, d_{min} is the minimum size of aggregate particle, V_a is the volume content of aggregate in concrete; V_{all} is the total volume of concrete.

After dividing the grading curve into different segments, it is possible to determine the size and number of aggregate particles by the grading segments containing the largest and smallest particles. For the grading segment $[d_s, d_{s+1}]$, the spherical aggregate particles can be generated in the following steps:

Step 1. Calculate the volume of aggregate $V_{agg}[d_s, d_{s+1}]$ to be generated in grading segment $[d_s, d_{s+1}]$ according to Fuller's grading curve.

Step 2. Generate a random diameter d within the segment $[d_s, d_{s+1}]$ to define the size of aggregate particles. It is assumed that the size d obeys uniform distribution between d_s and d_{s+1}, that is, $d_s \le d \le d_{s+1}$. It may also be expressed as $d = d_s + \eta (d_{s+1} - d_s)$, with η being a random number distributed uniformly between 0 and 1.

Step 3. Calculate the volume of the generated particles and subtract it from the aggregate volume $V_{agg}[d_s, d_{s+1}]$.

Step 4. Repeat Steps 2 and 3 until the remaining aggregate to be generated is less than $\pi d_s^3/6$. In other words, there is no more room to generate any aggregate particle in the current grading segment. Meanwhile, record the random number d ($d_s \le d \le d_{s+1}$) in a size array $Sz(i, s) = d$ (i = 1, 2, …, j), and the number of generated aggregate particles in a number array $Nb(s, 1) = j$. Next, transfer the volume of the remaining aggregate to the subsequent grading segment.

Step 5. Repeat all the steps above for the next smaller size grading segment until the generation of the last aggregate of the minimum particle size.

After obtaining the size and number arrays, select the near-spherical assemblies of elements to represent aggregates by replacing the properties of the mortar with those of the aggregates.

Once the size and corresponding number arrays have been ob-tained then the assemblies of elements which approximate spheres can be selected to represent aggregates by replacing the proper-ties of the cement mortar with those of the aggregates.

Generation of random aggregates and the ITZ

In numerical simulations, the concrete specimens are either cylindrical or cubic in shape, depending on the type of concrete materials. Here, the randomly generated aggregate particles are confined to cubic specimens. Two constraints were imposed to select assemblies of elements as aggregate particles at a free position within each concrete specimen: each assembly of elements must be completely within the boundary of the specimen, and no overlap is allowed with the previously selected assembly. The random aggregates and the ITZs were generated in the following procedure.

Step 1. Mesh the mortar of the specimen into regular solid hexahedral grids. The grid size should be determined on the accuracy requirements.

Step 2. Generate random coordinates (x, y, z) in 3D space within the specimen with the centre of the assembly of elements as aggregate.

Step 3. Check the central position against the previous selected size array $Sz(i, s)$ to see if both constraints are completely satisfied. If one of the two constraints is violated, do not select the assembly of elements as aggregate. Subsequently, repeat the coordinate generation and position check. By this analogy, select the assemblies of elements within $Nb(s, l)$ one by one.

Step 4. After the selection of all assemblies of elements within the grading segment $[d_s, d_{s+1}]$, change their material properties from mortar to aggregate. After that, proceed with the selection process in the subsequent grading segment.

Step 5. Repeat the steps above to select the assemblies of elements until all the assemblies of elements as aggregates are successively selected in the specimen and the total volume content of aggregates is satisfied.

Step 6. For each assembly of elements, select the outer surface nodes as aggregate, and split each node into two along the radial direction. Next, generate the ITZ elements between nodes and the corresponding new nodes. Moreover, reconstruct the mortar elements adjacent to aggregate by ERT without changing the material properties of these elements. Finally, check the quality of new elements and remove those failing the quality test (Fig. 2(e)).

Based on the given distribution of aggregate grading, a 3D meso-mechanical model (Fig. 2) was generated for concrete using the program developed by Xu et al. [28]. The randomly distributed unit set and near-spherical shape of aggregate completely

conform to the design requirements of the program. In addition, the ITZ was successfully generated through efficient and low-cost computation.

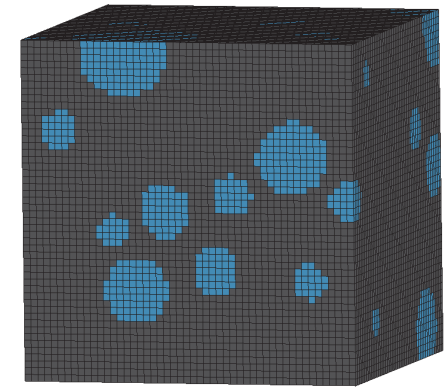

(a) concrete specimen.

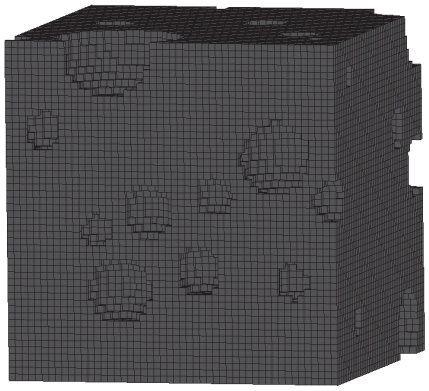

(b) cement mortar.

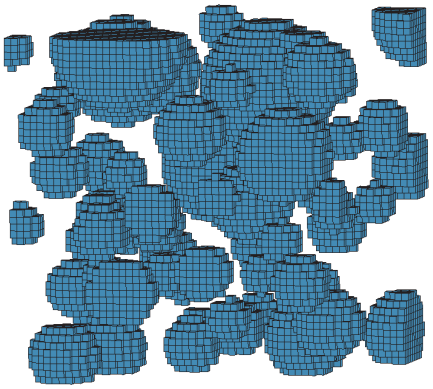

(c) aggregates.

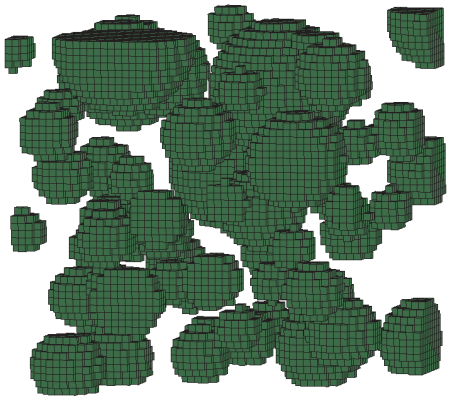

(d) interfacial transition zone (ITZ).

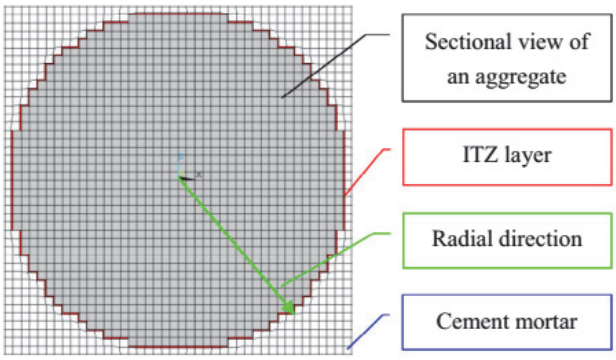

(e) partial enlarged sectional view of an aggregate with ITZ layer.

Figure 2: Schematic diagram of the 3D meso-mechanical model for cubed concrete specimen.

Contact definition and boundary conditions

During numerical calculation, the lower rigid plate was clamped and the speed direction of the upper rigid plate was perpendicular to the concrete specimen. There was no friction between the rigid plate and concrete specimen. To keep the element failure contact effective, the single-face automatic contact *CONTACT_AUTOMATIC_SINGLE_SURFACE was adopted for the simulation.

MATERIAL CONSTITUTIVE MODEL

The reliability of numerical simulation hinges on the feasibility of the numerical simulation model and the accuracy of the material constitutive model. As mentioned before, Liu Haifeng et al. [16-19] simulated the performance of concrete under dynamic load based on the HJC material constitutive model. However, the HJC takes no account of the damage evolution induced by the expansion of concrete volume, and its constitutive relation fails to describe the exact strain rate effect. In this paper, the mortar, aggregate and the ITZ are all illustrated by the concrete material constitutive model proposed by Xu and Wen. The model considers the following factors: the tensile and compressive damage effect, pressure correlation, Lode corner effect and strain rate effect. Since the material properties of the ITZ have not been fully understood, the material attribute of the ITZ was assumed to be the same of the mortar, except that its intensity is 60% of the latter. The relevant features of the material constitutive model are introduced as follows.

Pore state equation

The mortar, aggregate and the ITZ can be considered as porous materials. The pressure-volume strain relationship can be described by the pore state equation (i.e. $p\sim\alpha$ state equation). The volumetric strain of the fully compacted or solid materials can be expressed as [32]:

$$\bar{\mu}=\frac{\rho\alpha}{\rho_0\alpha_0}-1=\frac{\alpha}{\alpha_0}(1+\mu)-1 \tag{3}$$

where $\mu=\rho/\rho_0-1$ is the volumetric strain; ρ and ρ_0 are the current density and initial density, respectively; $\alpha=\rho_s/\rho$ and $\alpha_0=\rho_{s0}/\rho_0$ are the current porosity and initial porosity, respectively; ρ_s and ρ_{s0} are the current density and initial density of the solid material, respectively.

When $\bar{\mu}>0$, the concrete material belongs to the compressive state. The corresponding state equation can be expressed as:

$$\alpha=\max\left\{1,\min\left[\alpha_0,1+(\alpha_0-1)\left(\frac{p_{lock}-p}{p_{lock}-p_{crush}}\right)^n\right]\right\} \tag{4}$$

$$p=K_1\bar{\mu}+K_2\bar{\mu}^2+K_3\bar{\mu}^3 \tag{5}$$

where K_1, K_2 and K_3 are the bulk modulus of the solid material; p_{crush} is the pore collapse pressure under the load; p_{lock} is the pore densification pressure under the load.

When $\bar{\mu}<0$, the concrete material belongs to the tensile state. The corresponding state equation can be expressed as:

$$p=K_1\bar{\mu} \tag{6}$$

Intensity model

Considering the compressive and tensile damage effect of the material, the Lode angle effect, and strain rate effect [28-29, 33], the authors established the material constitutive relation to reveal the main mechanical features of concrete and other quasi-brittle materials based on the tripolar constrained face model. The intensity surface of concrete can be expressed according to the stress level on the material [29]:

$$Y=\begin{cases} 3\left(p+f_{tt}\right)r\left(\theta,e\right) & p<0 \\ \left[3f_{tt}+\left(f_{cc}-3f_{tt}\right)\times 3p/f_{cc}\right]r\left(\theta,e\right) & 0<p<f_{cc}/3 \\ \left[f_{cc}+Bf_c^{'}\left(p/f_c^{'}-f_{cc}/3f_c^{'}\right)^N\right]r\left(\theta,e\right) & p>f_{cc}/3 \end{cases} \tag{7}$$

where $f_{cc}=f_c^{'}DIF_{m\_t}\ \eta_c$ and $f_{tt}=f_tDIF_t\eta_t$; $f_c^{'}$ and f_t are respectively the static compressive strength and static tensile strength; DIF_{m_t} and DIF_t are respectively the dynamic compressive and tensile enhancement factors resulted from the strain rate effect; η_c and η_t are respectively the functions of shear damage and tensile softening of concrete [32-34]; B and N are empirical constants; $r(\theta, e)$ is the Lode corner effect [35], with θ and e being the ratio between the Lode angle and the tensile meridian and the ratio between the Lode angle and the compressive meridian, respectively.

As shown in Fig. 3, the strength surface of concrete can be classified into three segments: the tensile section ($p<0$), the transition section ($0<p<f_{cc}/3$) and the compressive section ($p>f_{cc}/3$).

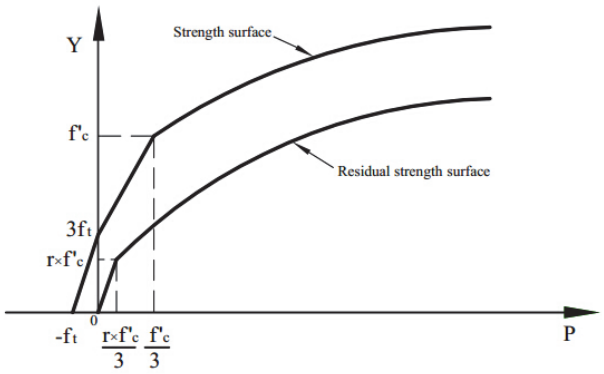

Figure 3: Strength surface of concrete

Parameters	Mortar	ITZ	Aggregate
ρ_0(kg/m^3)	2100	1800	2600
ρ_{s0}(kg/m^3)	2630	2630	2630
p_{crush}(MPa)	10.7	6.4	23.3
p_{lock}(GPa)	3	3	3
n	3	3	3
K_1(GPa)	14.2	6.9	17.4
K_2(GPa)	30	30	-3.0E3
μ	0.20	0.17	0.30
K_3(GPa)	10	10	1.5E5
G(GPa)	10.7	3.2	14.7
$f_c^{'}$(MPa)	32.0	19.2	70.0
f_t(MPa)	3.1	2.4	4.5
B	1.54	1.54	1.95
N	0.8	0.8	0.76

Table 1: Parameter values of the 3D meso-mechanical model.

Selection of material parameters

The model parameters of mortar, aggregate and the ITZ of this research are listed in Tab. 1. Specifically, the initial density ρ_0 of mortar and aggregate and the uniaxial compressive strength $f_c^{'}$ were extracted from Ref. [17]. The compaction density ρ_{s0} was set to 1.01 times of the initial density of aggregate. The uniaxial compressive strength $f_c^{'}$ and the elasticity modulus E of the ITZ were set to 60% of the mortar. The relevant parameter relations are as follows: $p_{crush}=f_c^{'}/3$, $K_1=E/3(1-2\nu)$, $G=E/2(1+\nu)$ and $f_t=0.54\sqrt{f_c^{'}}$. The values of the other parameters were obtained from Ref. [28].

NUMERICAL SIMULATION AND RESULTS ANALYSIS

Damage morphology

During the numerical simulation with our model, the aggregate volume content was 40% and the aggregate particle size fell in 5~20mm. The damage morphology of the cubic specimens with the side length of 150mm is presented in Fig. 4, where the grey white part is the removed unit. It can be seen that the specimens were basically destroyed along the ITZ. This phenomenon echoes with the theoretical results.

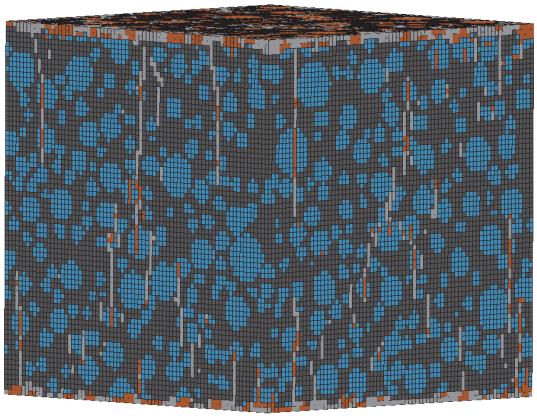

Figure 4: Damage morphology

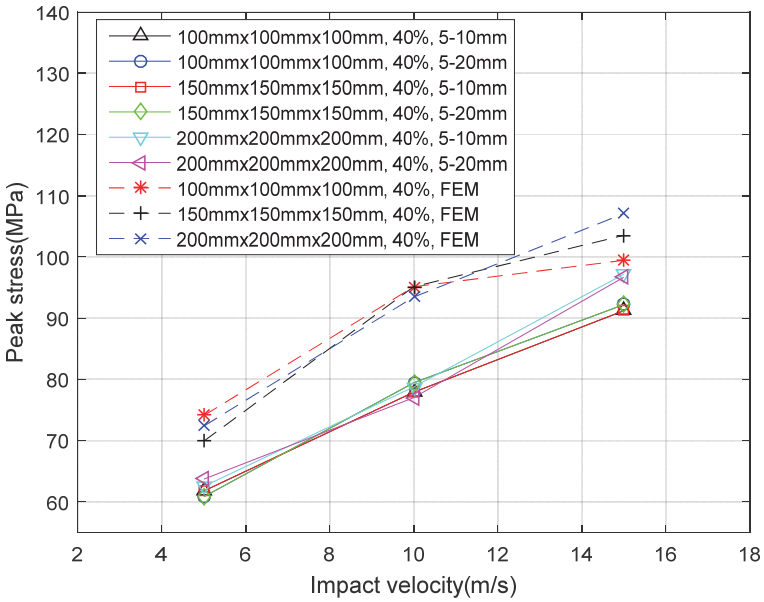

Figure 5: Relationship between the peak stress and the loading speed.

Effect of loading speed

The destruction of cubic concrete specimens (side length: 100mm, 150mm and 200mm; aggregate volume content: 40%; aggregate particle size: 5~10mm and 5~20mm) was simulated at different loading speeds. Then, the effect of the loading speed on peak stress of the concrete was analysed by the FEM and 3D micro model (Fig. 5).

As shown in Fig. 5, the peak stress gradually increased with the loading speed, whether it was 5m/s, 10m/s or 15m/s. This means the concrete is a sensitive material. Under the same condition, the peak stress of the 3D microscopic model is lower than that of the FEM, indicating that the former can reflect the inhomogeneity and low strength at the ITZ of the concrete. There were a large number of microcracks in the concrete. Some of them existed before the loading, and some were generated under the load. The original and load-induced microcracked grew steadily in different directions during the simulation. The interaction between the microcracks deflects the propagation direction, making it more time-consuming to achieve full penetration of the specimen.

At a low loading speed, the energy generated by the impact was rather small. This leaves enough time for the cracks to propagate and merge. In this case, only a few cracks extended and interacted with each other, resulting in a low stress level and a small peak stress. At a fast loading speed, the impact generated a huge amount of energy, leaving not enough time for stable cracks to propagate and merge. Thus, numerous microcracks extended almost simultaneously and interacted with each other. On the macroscale, the material withstood a rather high stress, i.e. the peak stress was on a high level.

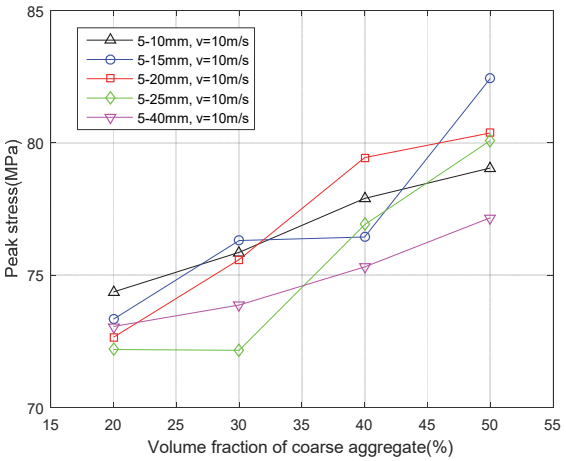

(a) 100mm×100mm×100mm specimen

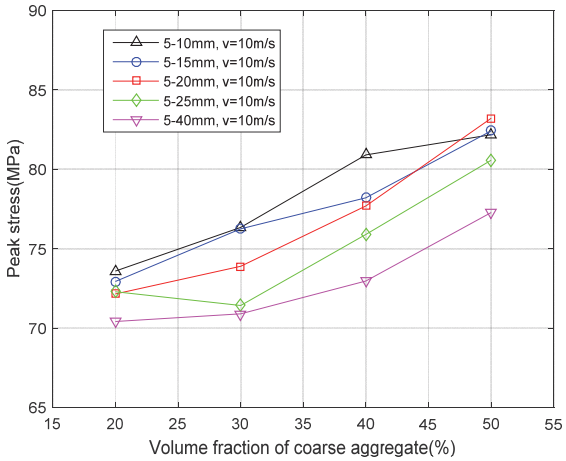

(b) 150mm×150mm×150mm specimen

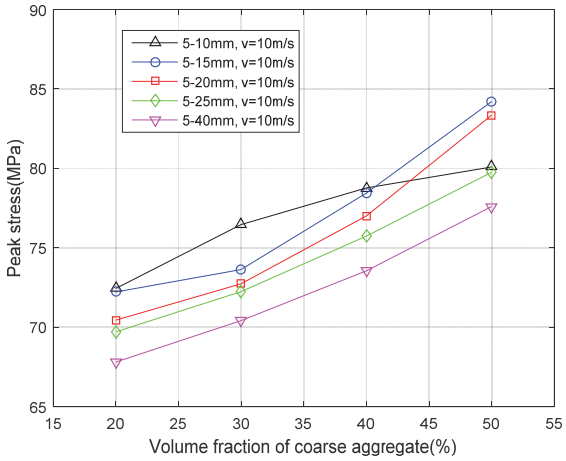

(c) 200mm×200mm×200mm specimen

Figure 6: Relationship between aggregate volume content and peak stress of concrete.

Effect of aggregate volume content

Keeping the loading speed at 10m/s, the destruction of cubic concrete specimens (side length: 100mm, 150mm and 200mm; aggregate particle size 5~10mm, 5~15mm, 5~20mm, 5~25mm and 5~40mm) was simulated at different aggregate volume contents. Then, the impact of aggregate volume content on the peak stress of concrete was deliberated in details (Fig. 6).

It can be seen from Fig. 6 that the peak stress increased continuously with the growth in aggregate volume content. This is because the volume of the mortar shrinks with the increase in aggregate volume; since the aggregate is much stronger than the mortar, the aggregate volume content exhibits a positive correlation with the concrete strength.

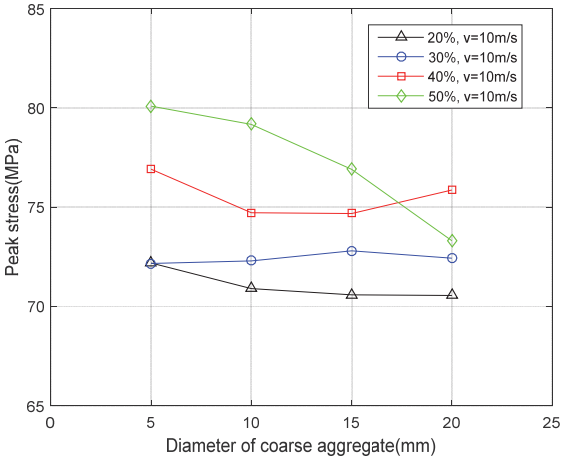

(a) 100mm×100mm×100mm specimen

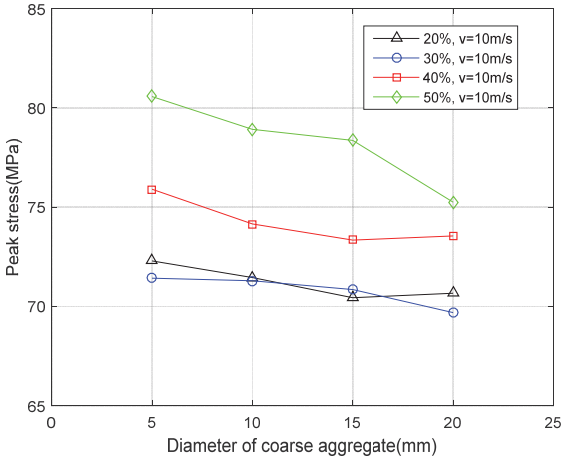

(b) 150mm×150mm×150mm specimen

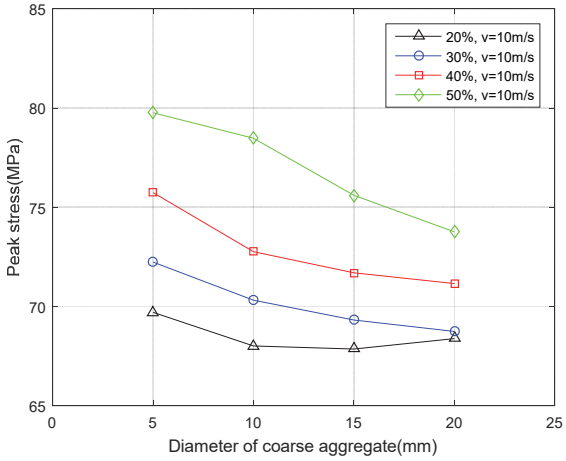

(c) 200mm×200mm×200mm specimen

Figure 7: Relationship between minimum aggregate particle size and peak stress of concrete.

Effect of minimum aggregate particle size

Under the constant loading speed (10m/s), aggregate grading and maximum aggregate particle size (25mm), the destruction of cubic concrete specimens (side length: 100mm, 150mm and 200mm; aggregate volume content: 20%, 30%, 40% and 50%) was simulated at different minimum aggregate particle sizes (5mm, 10mm and 15mm). Then, the impact of minimum aggregate particle size on the peak stress of concrete was discussed in details (Fig. 7).

It is clear that the peak stress was on the rise with the growth of aggregate volume content; when the aggregate volume content remained unchanged, the peak stress gradually declined with the increase in minimum aggregate particle size. The maximum value of the peak stress was observed at the aggregate particle size of 5mm. The overall decline of the peak stress under constant aggregate volume content can be explained as follows. First, it is more likely for aggregate particles to have internal defects if they are of a large size. Second, the specific surface area is small at a large minimum particle size, meaning

that less cement is needed to reach the same aggregate volume content; in this scenario, the binding area between the aggregate and the cement decreases, which weakens the ITZ and in turn the concrete.

Effect of maximum aggregate particle size

Under the constant loading speed (10m/s), aggregate grading and minimum aggregate particle size (5mm), the destruction of cubic concrete specimens (side length: 100mm, 150mm and 200mm; aggregate volume content: 20%, 30%, 40% and 50%) was simulated at different maximum aggregate particle sizes (10mm, 15mm, 20mm, 25mm and 40mm). Then, the impact of maximum aggregate particle size on the peak stress of concrete was analysed in details (Fig. 8).

It can be seen that the peak stress was on the rise with the growth of aggregate volume content; when the aggregate volume content remained unchanged, the peak stress gradually declined with the increase in maximum aggregate particle size. In other words, the peak stress exhibited a gradual declining trend with the growth in the maximum aggregate particle size, when the minimum aggregate particle size remained the same. This trend can be explained as follows. The specific surface area is small at a large maximum particle size, meaning that less cement is needed to reach the same aggregate volume content; in this scenario, a water film can develop easily on the aggregate surface, reducing the strength of the ITZ and adding to the mechanical nonuniformity of the concrete. Due to the porosity induced by the water film, the stress concentrates on the ITZ, which weakens the ITZ and in turn the concrete.

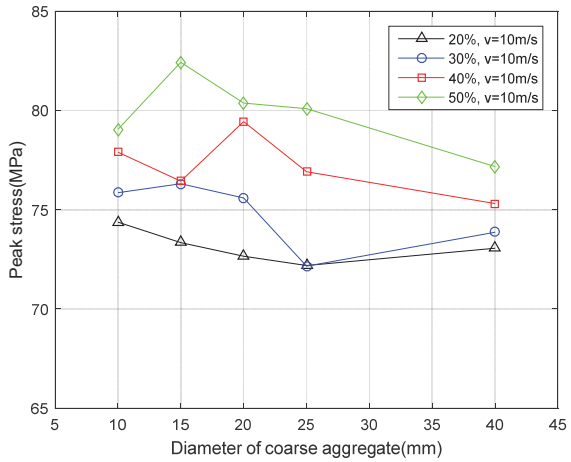

(a) 100mm×100mm×100mm specimen

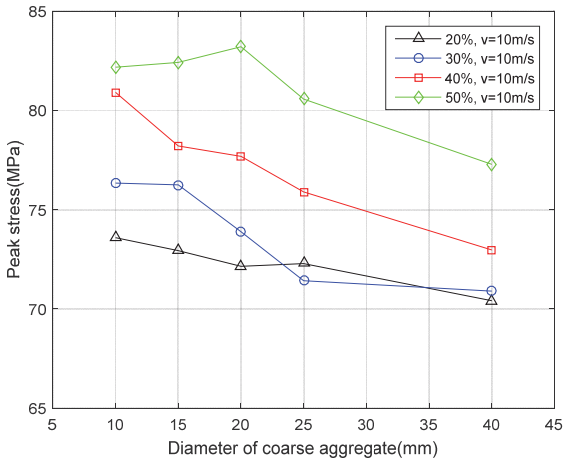

(b) 150mm×150mm×150mm specimen

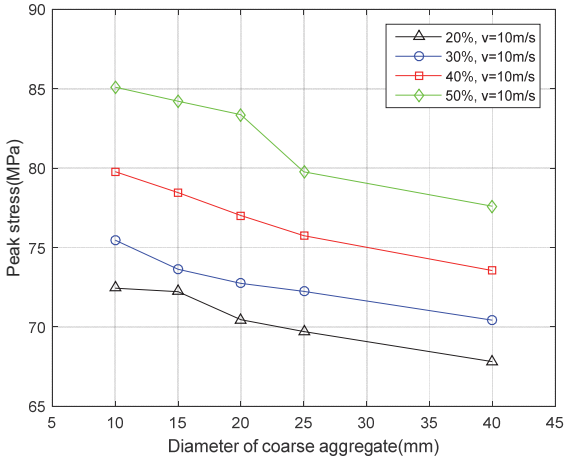

(c) 200mm×200mm×200mm specimen

Figure 8: Relationship between maximum aggregate particle size and peak stress of concrete

Conclusions

The dynamic load-induced response of concrete material is a rather complex process, involving the evolution of microdefects in the material, the sensitive effect of material strain rate, and the impact of hydrostatic pressure correlation and the Lode angle. Besides, the mechanical performance of concrete relies heavily on the size and distribution of the aggregate.

In view of these, this paper attempts to disclose the mechanical properties of concrete under dynamic load. To this end, concrete was considered as a three-phase composite of mortar, aggregate and the ITZ on the mesoscale. In light of the dynamic constitutive relation of concrete, the dynamic response of concrete specimens was numerically simulated on a 3D meso-mechanical model. Then, the authors discussed how the loading speed, aggregate volume content, and aggregate particle size affect the dynamic mechanical properties of concrete. The simulation results show that the damage morphology of concrete under dynamic load agrees well with that of theoretical analysis; the peak stress of concrete increased with the loading speed; the peak stress of concrete also increased with aggregate volume content; however, the peak stress of concrete gradually decreased with the increase in aggregate particle size under the constant volume content and grading of aggregate. The research findings shed new light on anti-impact design of concrete structures.

Acknowledgments

The research of this paper is made possible by the generous support from The National Natural Science Foundation of China (Grant No: 51678221); Key Project of Natural Science Research in Anhui Universities (Grant No: KJ2017A405); Natural Science Research Project of West Anhui University (Grant No: WXZR201615; WXZR201626; 2010LW009; KJ103762015B12).

References

[1] Bischoff, P.H. and Perry, S.H. (1991). Compressive behaviour of concrete at high strain rates, Materials and structures, 24, pp. 425-450.

[2] Gary, G. and Bailly, P., (1998). Behaviour of quasi-brittle material at high strain rate. Experiment and modelling, European Journal of Mechanics-A/Solids, 17, pp. 403-420.

[3] Geng, B.Y., Ni, W., Wu, H., Huang, X.Y., Cui, X.W., Shuang, Wang, S. and Zhang, S.Q. (2016). On high-strength low-shrinkage ITOs-based concrete, International Journal of Heat and Technology, 34, pp. 677-686.

[4] Brara, A., Camborde, F., Lepaczko, J.K. and Mariotti, C. (2001). Experimental and numerical study of concrete at high strain rates in tension, Mechanics of materials, 23, pp. 33-45.

[5] Pedersen, R.R., Simone, A. and Sluys, L.J. (2013). Mesoscopic modeling and simulation of the dynamic tensile behavior of concrete, Cement and Concrete Research, 50, pp.74-87.

[6] Schlangen, E. and Garboczi, E.J. (1997). Fracture simulations of concrete using lattice models: computational aspects, Engineering fracture mechanics, 57, pp. 319-332.

[7] Li, G.L. and Mier, J.G. (2003). 3D lattice type fracture model for concrete, Engineering Fracture Mechanic, 70, pp. 927-941.

[8] Cundall, P.A., Strack, O.D. (1979). A discrete numerical model for granular assemblies, Geotechnique, 29, pp. 47-65.

[9] Bažant, Z.P., Tabbara, M.R., Kazemi, M.T. and Pijaudier-Cabot, G. (1990). Random particle model for fracture of aggregate or fiber composites, Journal of engineering mechanics, 116, pp. 1686-1705.

[10] Liu, G.T. and Wang, Z.M., (1996). Numerieal simulation study of fraeture of concrete materials using random aggrega model, Journal of Tsinghua University (Science and Technology), 36, pp. 84-89.

[11] Wang, Z., Kwan, A. and Chan, H., (1999). Mesoscopic study of concrete I: generation of random aggregate structure and finite element mesh, Computers & Structures, 70, pp. 533-544.

[12] Zhu, W. and Tang, C., (2002). Numerical simulation on shear fracture process of concrete using mesoscopic mechanical model, Construction and Building Materials, 16, pp. 453-463.

[13] Zhu, W., Tang, C. and Wang, S., (2005). Numerical study on the influence of mesomechanical properties on macroscopic fracture of concrete, Structural Engineering and Mechanics, 19, pp. 519-534.

[14] Song, J. and Chen, F.Y. (2015). Calculation model for thermo-mechanical coupling and 3D numerical simulation for concrete tower of cable-stayed bridge, Mathematical Modelling of Engineering Problems, 2, pp. 9-12.
[15] Liu, H.F. and Ning, H.F. (2012). Constitutive model for concrete subjected to impact loading, Journal of Southeast University, 28, pp. 79-84.
[16] Zhang, H.Y., (2015). Thermodynamic property of concrete and temperature field analysis of the base plate of intake tower during construction period, International Journal of Heat and Technology, 33, pp. 145-154.
[17] Liu, H.F. and Han, L. (2016). Numerical Simulation of Dynamic Mechanical Behavior of Concrete with Two-dimensional Random Distribution of Coarse Aggregate, Chinese Journal of High Pressure Physics, 30, pp. 191-199.
[18] Liu, H.F. and Ning, J.G. (2009). A meso-mechanical constitutive model of concrete subjected to impact loading, Explosion and Shock Waves, 29, pp. 2261-267.
[19] Liu, H.F., Wang, Y.Y. and Song, J.X. (2016). Numerical simulation of dynamic mechanical behaviors of desert sand concrete, Journal of Hydraulic Engineering, 47, pp. 493-500.
[20] Du, X.L., Tian, R.J., Peng, Y.J. and Tian, Y.D. (2009). Numerical simulation of concrete dynamic compressive strength under impact loading based on mesomechanics, Journal of Beijing University of Technology, 35, pp. 213-217.
[21] Du, X.L. and Jin, L. (2011). Mechanical property reserch on concrete based on random multi-scale mechanical model, Engineering Mechanics, 28, pp. 151-155.
[22] Ren, W.Y., Yang, Z.J. and Huang, Y.J. (2015). Meso-scale fracture modelling of concrete based on X-ray computed tomography images, Journal of Hydraulic Engineering, 46, pp. 452-459.
[23] Park, S.W., Xia, Q. and Zhou, M. (2001). Dynamic behavior of concrete at high strain rates and pressures: II. Numerical simulation, International journal of impact engineering, 25, pp. 7887-7910.
[24] Wang, Z.M. and Qiu, Z.Z. (2005). Random aggregate structure of mesoscopic concrete and finite element mesh, Chinese Journal of Computational Mechanics, 22, pp. 728-732.
[25] Xu, H. and Wen, H.M. (2016). A computational constitutive model for concrete subjected to dynamic loadings ,2016, International Journal of Impact Engineering, 91, pp. 116-125.
[26] Song, L.Z., Shen, T. and Yu, B. (2013). The approach to establishing a two-dimensional parameterized aggregate model for concrete simulation, Engineering Mechanics, 30, pp. 5-13.
[27] Zhang, Z.H., Zhao, H. and Yu, H. (2011). Experimental and numerical Simulation of concrete dynamic mechanical properties, Chinese Journal of High Pressure Physic, 25, pp. 533-538.
[28] Xu, P.B., Xu, H. and Wen, H.M. (2016). 3D meso-mechanical modeling of concrete spall tests, International Journal of Impact Engineering, 97, pp. 46-56.
[29] Xu, H. and Wen, H.M. (2016). A computational constitutive model for concrete subjected to dynamic loadings, International Journal of Impact Engineering, 91, pp. 116-125.
[30] Riggers, P. and Moftah, S.O. (2006). Mesoscale models for concrete: Homogenisation and damage behaviour, Finite elements in analysis and design, 42, 623-636.
[31] Hao, Y., Hao, H. and Zhang, X. (2012). Numerical analysis of concrete material properties at high strain rate under direct tension, International Journal of Impact Engineering, 39, pp. 51-62.
[32] Hartmann, T., Pietzsch, A. and Gebbeken, N. (2010). A hydrocode material model for concrete, International Journal of Protective Structures, 4, 443-468.
[33] Xu, H. and Wen, H. (2013). Semi-empirical equations for the dynamic strength enhancement of concrete-like materials, International Journal of Impact Engineering, 60, pp. 6-81.
[34] Malvar, L.J., Crawford, J.E., Wesevich, J.W. and Simons, D. (1997). A plasticity concrete material model for DYNA3D, International Journal of Impact Engineering, 19, pp. 847-873.
[35] William, K. and Warnke, E., (1975). Constitutive model for the triaxial behavior of concrete, International Association for Bridge and Structural Engineering, Bergamo, Italy.